


Strongly correlated electrons in the ferroelectric metal LiOsO₃J.-S. Zhou ^{*}, X. Li , J. M. He , and J. Chen *Materials Science and Engineering Program, Mechanical Engineering, University of Texas at Austin, Austin, Texas 78712, USA*K. Yamaura *International Center for Materials Nanoarchitectonics (WPI-MANA), National Institute for Materials Science, 1-1 Namiki, Tsukuba, Ibaraki 305-0044, Japan
and Graduate School of Chemical Sciences and Engineering, Hokkaido University, North 10 West 8, Kita-ku, Sapporo, Hokkaido 060-0810, Japan*

(Received 25 June 2021; revised 25 August 2021; accepted 8 September 2021; published 17 September 2021)

The metallic LiOsO₃ undergoes a transition to a polar phase below $T_s \approx 140$ K. This unusual property provides a unique opportunity to study the interaction between free electrons and electric dipoles. We report a suite of measurements of physical properties in LiOsO₃ as a function of temperature, including resistivity and magnetoresistance down to 0.16 K, thermoelectric power, high-precision magnetization, specific heat, and thermal conductivity on textured single-crystal samples. Enhancements from the electron contribution to the specific heat and the paramagnetic susceptibility indicate that electrons in LiOsO₃ are highly correlated. An anomalously large Kadowaki-Woods ratio also supports the argument of strongly correlated electrons in LiOsO₃. In the nonpolar phase above T_s , electrons are coupled strongly to the lattice vibrations, which leads to the resistivity saturation at high temperatures and eventually a crossover to the hopping conduction. The data of thermal conductivity and specific heat are consistent with an order-disorder transition at T_s . The analysis of critical behavior in the resistivity, specific heat, and the thermal conductivity provides useful information for understanding the electron-dipole interaction in LiOsO₃.

DOI: [10.1103/PhysRevB.104.115130](https://doi.org/10.1103/PhysRevB.104.115130)**I. INTRODUCTION**

Almost all ferroelectrics are insulators. Ferroelectricity arises due to a long-range dipole-dipole interaction [1]. Metallicity and ferroelectricity are seemingly incompatible since free electrons screen dipole-dipole interaction. The transition to a polar phase is possible in a metal if free electrons do not interact strongly with the transverse optical phonons. This possibility was postulated by Anderson and Blount [2] when they studied the martensite transition in V₃Si. The discovery of the polar metal LiOsO₃ [3] revived interest on this subject. It has been recognized that LiOsO₃ fulfills the definition of a ferroelectric metal given by Anderson and Blount [2,4]. The possible interplay among electron-dipole interaction, electron-phonon interaction, Hund's coupling, spin-orbit coupling, and electron-electron interaction in LiOsO₃ also triggered computational and theoretical studies [5–11]. However, issues such as whether electron-phonon interaction is weak in LiOsO₃, which allows the ferroelectric transition as proposed by Anderson and Blount [2]; whether LiOsO₃ is a strongly correlated system; and whether the nonpolar-to-polar transition alters the band structure for the states near the Fermi energy are still controversial. LiOsO₃ is a metal from 300 to 2 K. At low temperatures, the $\rho(T)$ exhibits a power law dependence, and the residual resistivity is significantly

large. The polar-to-nonpolar transition at $T_s = 140$ K leads to a sign change of the curvature in $\rho(T)$; the resistivity saturates quickly for $T > T_s$ [3]. The Raman study on a LiOsO₃ crystal verified a second-order phase transition at T_s [12]. By tracking down a Raman active mode 3E_g , Jin *et al.* [13] can extract important information about dynamics of the A_{2u} mode associated with Li displacement near T_s and the critical behavior at the transition. The data allowed them to derive a strong electron-phonon coupling which seems contradictory to the assumption made by Anderson and Blount [2] for a ferroelectric metal. In the same report, the authors have measured the Hall coefficient. The data indicate an anisotropic scattering that increases, especially at $T < T_s$, with decreasing temperature. In contrast, a study with a terahertz pump-probe on LiOsO₃ concluded that the itinerant electrons are decoupled from the soft transverse optical phonons [14]. The Raman study indicates negligible critical fluctuations in the vicinity of nonpolar-to-polar transitions. This observation appears to be inconsistent with the conclusion from an optical study with second-harmonic generation (SHG) [15]. LiOsO₃ is a bad metal as characterized by infrared spectroscopy, which shows a small quasiparticle spectral weight in the energy range from the Drude analysis, a clear sign for being close to a Mott-Hubbard transition [16]. However, there are no clear signatures for a strongly correlated system from the reported results of transport and magnetic properties of LiOsO₃. Moreover, whether LiOsO₃ can become superconducting at low temperatures as predicted by Anderson and Blount [2] for

^{*}Corresponding author: jszhou@mail.utexas.edu

a ferroelectric metal remains unclear. The nonpolar-to-polar phase transition in LiOsO_3 changes the phonon structure. It remains unknown how the phonon structural change influences the thermal transport property. A careful comparative study between LiOsO_3 and other ferroelectric metals has not been made. This paper aims to address these questions.

In comparison with the electron-electron interactions, electron-phonon interactions, and electron-magnon interactions, the interaction between free electrons and dipoles has been rarely studied since few ferroelectric systems are conducting. In the conductor $\text{Pb}_{1-x}\text{Ge}_x\text{Te}$, the off-center Ge ions form an electric dipole that interacts with free electrons. The two-level system model developed by Katayama *et al.* [17] can account for the anomalous logarithmic increase of resistivity at low temperatures. The presence of free electrons in turn influences the dipole-dipole interaction V_{dd} , i.e., V_{dd} having alternating sign as a function of R (the distance between dipoles) like the Ruderman-Kittel-Kasuya-Yosida (RKKY) interaction. The tendency to have free electrons in dipole systems is to promote the dipole glass state instead of long-range ordering [18].

SrTiO_3 is well-known for quantum ferroelectric since it is at the tipping point for a ferroelectric transition [19]. The cubic perovskite exhibits a ferroelectric transition for the ^{18}O -enriched sample. Ferroelectricity can also be induced in a very narrow range ($0.0018 < x < 0.02$) of the Ca doping in $\text{Sr}_{1-x}\text{Ca}_x\text{TiO}_3$. The ferroelectric transition survives in the metallic phase $\text{Sr}_{1-x}\text{Ca}_x\text{TiO}_{3-\delta}$ with oxygen deficiency [20]. As in $\text{Pb}_{1-x}\text{Ge}_x\text{Te}$, the ferroelectric transition triggers a resistivity upturn in $\text{Sr}_{1-x}\text{Ca}_x\text{TiO}_{3-\delta}$. The authors adopted the same dipole version of the RKKY interaction to account for the resistivity anomaly.

The ferroelectric metal (with the definition by Anderson and Blount [2]) LiOsO_3 is dramatically different from the systems above. (1) The density of off-center ions, i.e., the density of dipoles, is extremely low in $\text{Pb}_{1-x}\text{Ge}_x\text{Te}$ and $\text{Sr}_{1-x}\text{Ca}_x\text{TiO}_{3-\delta}$ in comparison with that in LiOsO_3 . (2) On cooling, the ferroelectric transition triggers a drop of resistivity in LiOsO_3 instead of an upturn in $\text{Pb}_{1-x}\text{Ge}_x\text{Te}$ and $\text{Sr}_{1-x}\text{Ca}_x\text{TiO}_{3-\delta}$. (3) LiOsO_3 is not a regular metal as seen from the resistivity saturation above T_s . (4) The interaction between free electrons and dipoles appears to enhance long-range dipole ordering. (5) Most importantly, electrons in LiOsO_3 are strongly correlated, as demonstrated in this paper. How to treat the interplay between electron-electron interactions and electron-dipole interaction is an interesting topic in condensed matter physics; LiOsO_3 is a unique system for the study.

II. TRANSPORT PROPERTIES

The samples used in this paper were synthesized under high pressure in Japan and in the U.S. The detail of high-pressure synthesis can be found in a previous report [3]. Osmium metal is stable in dry air. However, OsO_2 may react with oxygen in air to form extremely toxic OsO_4 . All high-pressure assemblies were prepared in a glovebox with pure Ar (with O_2 and H_2O in 0.1 ppm). The high-pressure product LiOsO_3 with Os^{5+} is stable in air, as checked over time with x-ray powder diffraction. Measurements of resistivity

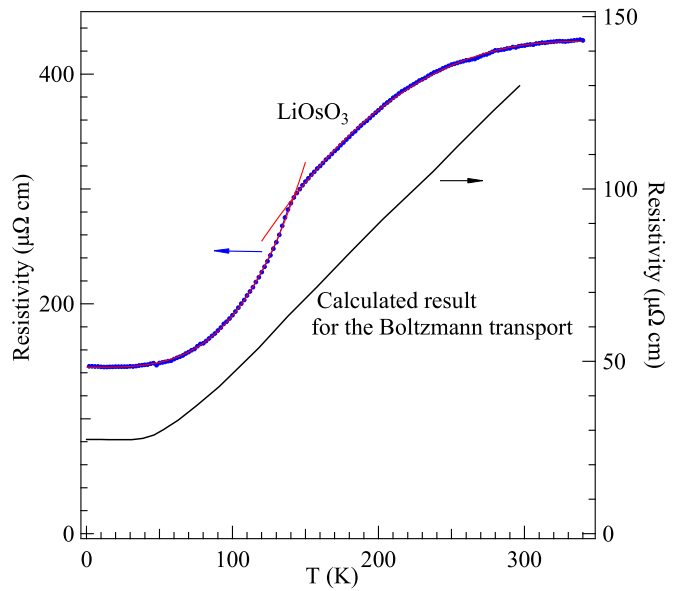


FIG. 1. Temperature dependence of resistivity of LiOsO_3 crystal. Lines in the plot are from the fitting to power laws, see the text for details. The resistivity data with scale on the right side of vertical axis are from the calculation in studying the transport property of SrRuO_3 [21]. The calculated result is used to show the typical behavior of a metal that can be accounted for by the Boltzmann model.

$\rho(T)$ were made on needle-shaped crystals with a $\sim 150 \mu\text{m}$ length and a $20\text{--}30 \mu\text{m}$ cross section, which are not oriented. Measurements of the thermoelectric power were made on pellets consisting of textured crystals with both the thermal transport option in a Physical Property Measurement System (PPMS) from Quantum Design and a homemade system. Several pieces of crystals from two batches of high-pressure synthesis were measured. Essential features of $\rho(T)$ and $S(T)$ are highly reproducible, and the residual resistivity values in these crystals fall in a narrow range. Some crystals show a loop of $\rho(T)$ around T_s between the cooling down and warming up runs, which can be attributed to the crystal crack at the domain boundaries during the thermal cycles. These loops have never been observed in $S(T)$, which confirms the grain boundary effects in origin. In comparison with the resistivity data reported previously [3], the resistivity measurement in this paper was made over a much wider temperature range 0.16–360 K. Moreover, the residual resistivity of crystals from two different batches of LiOsO_3 is generally smaller than that in the reported data [3].

Figure 1 displays a typical result of $\rho(T)$ measured on the LiOsO_3 crystal. The transition to a polar phase on cooling through T_s causes an abrupt drop of resistivity. The $\rho(T)$ in both the nonpolar and polar phases deviates from our understanding for a regular metal. For a regular metal, the temperature dependence of resistivity can be described by the Boltzmann gas model with the electron-phonon interaction; examples of regular metals include ReO_3 , BaPbO_3 , CoSi , and Pd_2Si [22]. A Bloch-Grüneisen curve of the resistivity in studying SrRuO_3 is superimposed in Fig. 1, which is roughly a power law $\rho \sim T^5$ at low temperatures and a linear relationship $\rho \sim T$ at high temperatures. These features can be found in the metals listed above but appear to be missed in

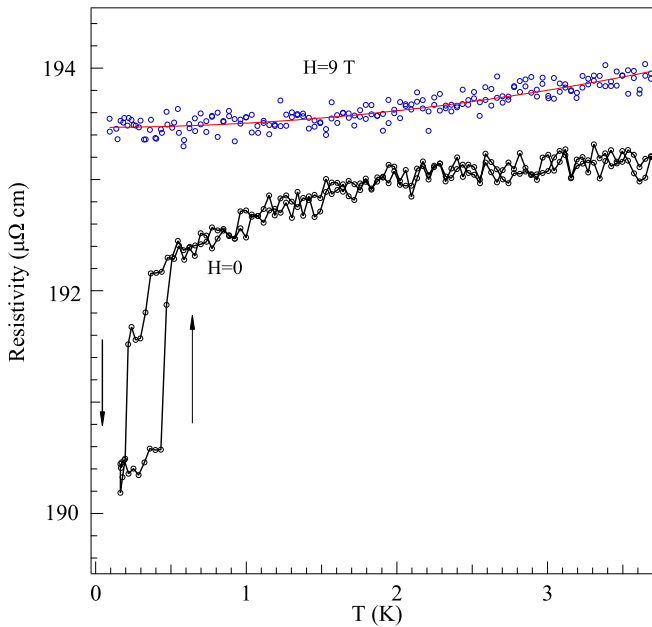


FIG. 2. Temperature dependence of resistivity for LiOsO₃ crystal at low temperatures. The line in $\rho(T)$ under 9 Tesla is the fitting result to a power law $\rho(T) = \rho_0 + AT^n$, see the text for the discussion about the fitting result.

the $\rho(T)$ of LiOsO₃. The residual resistivity ρ_0 of LiOsO₃ is unusually high. The $\rho(T)$ for the entire temperature range in this paper can be fit to the power laws $\rho \sim T^{3.4}$ for $T < T_s$ and $\rho \sim (340 - T)^{2.37}$ for $T > T_s$. The resistivity measurements on two LiOsO₃ single crystals were made down to 160 mK with a dilution refrigerator in the PPMS; the results are identical, and the $\rho(T)$ of one crystal is shown in Fig. 2. Results shown in Figs. 1 and 2 were measured on different crystals; the offset of the resistivity at 2 K between the results in Figs. 1 and 2 can be attributed to the measurement uncertainty of the dimension of the sample and the distance between voltage leads. The abrupt drop of the resistivity at $T \approx 0.2$ K appears to be related to a superconducting transition of the Os metal [23] since high-resolution synchrotron powder diffraction on the powder sample made by pulverizing the crystal reveals a small amount of Os metal phase. The filamentary Os metal phase does not establish a percolation connection through the crystal. Therefore, $\rho(T)$ only shows a small drop at the superconducting transition temperature of the Os metal. The superconducting origin of the resistivity anomaly is further confirmed by the measurement with a magnetic field $H = 9$ T. The resistivity anomaly together with an obvious resistivity reduction in the vicinity of sub-Kelvin due to pairing fluctuations is fully removed under $H = 9$ T. A small magnetoresistance (MR) effect at $T > 0.2$ K is understandable based on Kohler's rule for a metal. We have fit $\rho(T)$ at 9 Tesla to a power law $\rho(T) = \rho_0 + AT^n$ with $n = 1.98 \pm 0.26$. The effect of electron-phonon interactions is much smaller than electron-electron interactions at low temperatures. The fitting parameter $n \approx 2$ indicates a Landau-Fermi liquid behavior in the polar phase of LiOsO₃ at low temperatures. Another fitting parameter A will be used for the Kadowaki-Woods ratio that is discussed with the specific heat result.

It should be noticed that LiOsO₃ shows an unusually high residual resistivity ρ_0 obtained by extrapolating the $\rho(T)$ at 9 T to 0 K, in which the resistivity change due to any filamentary superconductivity is removed. Electric resistivity in a metal is caused by electrons interacting with lattice vibrations and defects. Thermal vibrations scatter electrons, which can be treated with the Boltzmann gas model. At 0 K, the resistivity comes from scattering on defects. A large residual resistivity may be the intrinsic property of the oxide. Li ions are at $6a$ position $(0,0,z)$ and $(0,0,z + \frac{1}{2})$ in the LiNbO₃ structure with the space group $R3c$. The ferroelectric displacement originates from Li moving along the z axis. The thermal displacement factor β_{33} for the Li site increases drastically on cooling through T_s and remains large to the lowest temperature [3]. A larger thermal displacement factor at low temperatures indicates some randomness of Li displacement along the z direction, which contributes the scattering to free electrons and should be the primary source for a large residual resistivity.

Whereas the curvature of $\rho(T)$ at $T < T_s$ is the same as the prediction from the Boltzmann gas model, the power-law dependence $\rho \sim T^{3.4}$ to 140 K differentiates LiOsO₃ from a regular metal. Here, T_s marks a sign change of the curvature of $\rho(T)$, which results in a resistivity saturation at $T > T_s$. With a partially filled t_{2g} orbital in the low spin Os⁵⁺, LiOsO₃ could be a good candidate for a Hund's metal. In a Hund's metal, electron hopping between atoms has the penalty of J_H if the spin state at the receiving atom violates Hund's rule in addition to the onsite Coulomb energy [24]. Mixing of J_H into a strongly correlated system leads to a distinct feature in resistivity. The theory predicts a characteristic temperature T^* which is proportional to the Drude weight in a metallic system. Here, T^* separates a coherent state at low temperature described by the Fermi liquid state and incoherent state at high temperatures which shows a $\rho(T)$ with intending saturation as temperature increases [24]. The resistivity of iron pnictide KFe₂As₂ fits the description of a Hund's metal well [25]. Back to LiOsO₃, the remarkable sign change of the curvature at T_s may suggest the transition at T_s coincides with a coherence-incoherence crossover as in a Hund's metal. Recent theoretical work has shown that the electronic state in LiOsO₃ is close to a Hund's-Mott insulator transition and predicted a crossover from a metallic to an incoherent behavior [10].

On the other hand, the $\rho(T)$ of LiOsO₃ at high temperatures resembles the resistivity saturation found in an A15 compound [26]. Theories to rationalize this behavior evolved over time. The early model states that resistivity deviates from the prediction of the gas model as the electron mean free path is close to the lattice parameter. A more convincing model to describe the phenomena is that the electron-phonon interaction is so strong that the Migdal approximation, one of the key requisitions to make the gas model work, is no longer valid [27]. The resistivity saturation is the sign of a smooth crossover from electron scattering to electron hopping. This scenario appears to fit the case of LiOsO₃. We have indeed observed a resistivity decrease with increasing temperature at $T > 360$ K (not shown in Fig. 1). A strong electron-phonon interaction based on the scenario above is consistent with the conclusion from a Raman study on LiOsO₃ [13]; the study also gives a microscopic picture of how electrons couple with dipoles. The crossover from electron scattering to electron

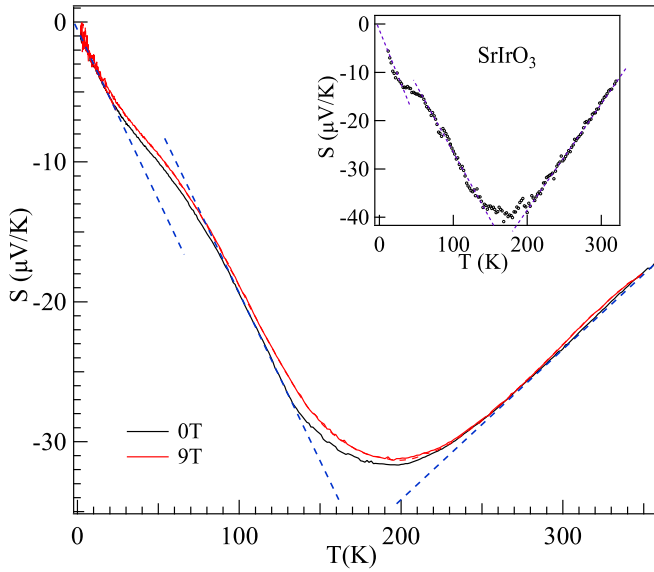


FIG. 3. Temperature dependence of the thermoelectric power for LiOsO₃; lines inside the plot are guides to eyes. Inset: Temperature dependence of the thermoelectric power for perovskite SrIrO₃ [30]. SrIrO₃ also shows an anomalous thermoelectric power, i.e., a hump (of magnitude) ~ 180 K, which is stunningly like the $S(T)$ of LiOsO₃.

hopping at high temperatures and the conclusion from the Raman study in LiOsO₃ [13] are inconsistent with the mechanism of ferroelectric metal by Anderson and Blount [2], which is based on a weak electron-transverse phonon coupling. The real driving force for the transition to a polar phase in LiOsO₃ deserves further study. A drastic increase of T_s under pressure [28,29] and the corresponding change in the structure [29] indicate that the local structural instability may be the driving force for the transition to a polar phase at T_s .

Figure 3 displays the result of thermoelectric power S ; it is highly repeatable on several textured LiOsO₃ crystals. The overall negative S indicates that LiOsO₃ is an electronic conductor, which is consistent with the Hall coefficient measurement [13]. A broad maximum of $|S|$ occurs at 200 K followed by a nearly linear decrease of $|S|$ as temperature approaches 0 K. In the measurement for testing the magnetic field dependence of the thermoelectric power, the contribution from the Nernst effect has been ruled out since resulting $S(T)$ with $\pm H$ are overlapped. The magnitude of S is slightly suppressed under magnetic field $H = 1$ T in the temperature range $100 < T < 220$ K, and no field dependence is found for $H > 1$ T (up to 9 T) in comparison with S at $H = 1$ T; $S(T)$ for $H = 9$ T is shown in Fig. 3.

The thermoelectric power in a metal can be treated roughly as the electronic contribution to specific heat per electron, i.e., $S \approx C_{el}/e = (\gamma/e)T$, which provides a good explanation of the linear decrease of $|S|$ in LiOsO₃ as T approaches 0 K. Electrons are scattered by impurities and lattice vibrations in a solid. In the temperature range $T \geq \theta$ or $T \ll \theta$, θ is the Debye temperature, the thermoelectric power is dominated by electron-impurity scattering. In this case, S can be expressed by the diffusive formula $S = (\frac{\pi^2 k^2}{eE_F})T$ for $T \ll \theta$ [31]. Taking $E_F \approx 2$ eV from the band calculation for LiOsO₃ [3], $S = -0.037T(\mu\text{V}/\text{K})$ is obtained; the absolute value of the slope

0.037 is much smaller than $0.23 \mu\text{V}/\text{K}^2$ obtained by fitting the $S(T)$ at $T < 25$ K in Fig. 3. The diffuse formula $S = (\frac{\pi^2 k^2}{eE_F})T$ is derived on an assumption of a sphere Fermi surface. The ferroelectric LiOsO₃ must have a much more distorted Fermi surface. A general expression of S is needed to understand the profile of S with the E_F at different locations in a band:

$$S = \frac{\frac{1}{eT} \int (E - E_F) \sigma(E) \frac{\partial f_0}{\partial E} dE}{\int \sigma(E) \frac{\partial f_0}{\partial E} dE}, \quad (1)$$

where $\sigma(E)$ is defined by $\sigma = \int \sigma(E) dE$, and f_0 is the Fermi-Dirac distribution function. The thermoelectric power is a measure of the asymmetry of the energy dependence conductivity crossing the Fermi energy. For a single band system, a large $|S|$ is expected to occur for the E_F located in the top or bottom of the band. Both LiOsO₃ and NaOsO₃ have the t_{2g}^3 electronic configuration. These systems with the Fermi energy located in the middle of the π^* band consisting of highly hybridized O : $2p$ and Os : $5d$ orbitals are expected to exhibit a small and weak temperature-dependent S . Here, $S(T)$ of NaOsO₃ (unpublished) at temperatures above the metal-insulator transition fulfills this expectation. A large $|S|$ of LiOsO₃ can be attributed to the peculiar electron density of state (DOS) in the $R3c$ structure. A pronounced minimum below E_F within 0.5 eV [3] effectively makes the E_F of LiOsO₃ at the bottom of a band, which gives rise to a negative S with a large magnitude in LiOsO₃.

In a typical broadband metal like copper, the electron-phonon interaction manifests as the phonon-drag effect in the thermoelectric power, which is normally present as a broad hump in S at $T \sim \theta/4$, θ is the Debye temperature [31]. The physics of the phonon-drag effect is that, in addition to the electron diffusion driven by the temperature gradient, the travel of phonons with a long mean free path adds a driving force on electrons, so that the drag effect would have the temperature dependence of $1/T$. At low temperatures, a fast reduction of the phonon population makes the effect vanishing in T [3]. Therefore, the phonon-drag effect essentially resembles the temperature dependence of phonon thermal conductivity. Given a θ in the range 155–675 K, depending on temperature from the specific-heat measurement and a broad peak in the thermal conductivity discussed in a following section, a hump in $S(T)$ at 30 K is expected. Whereas $S(T)$ of LiOsO₃ in Fig. 3 deviates from a linear behavior ~ 30 K, the essential feature of a typical phonon-drag effect is missing here. In a narrow band system, an enhanced electron-phonon coupling reduces significantly the phonon mean free path. As a result, the phonon-drag effect is suppressed. A good example can be found in La_{1-x}Nd_xCuO₃ [32]. The bandwidth is progressively reduced with increasing of the Nd substitution, which bends the Cu-O-Cu bond angle from 180° in this rhombohedral perovskite structure. The phonon-drag effect found in LaCuO₃ is gradually reduced and vanishes as x increases in La_{1-x}Nd_xCuO₃. Missing the phonon-drag effect in LiOsO₃ signals strongly correlated electrons. We will come back to this point when we discuss the data of specific heat and magnetic susceptibility.

Another important feature in $S(T)$ of LiOsO₃ is that T_s separates a roughly linear temperature dependence $S \sim T$ in the polar phase at $T < T_s$ from a highly unusual $S(T)$ in the

nonpolar phase at $T > T_s$. While much enhanced, the linear temperature dependence of $S(T)$ at $0 < T < 25$ K and $70 < T < 140$ K and the monotonic increase of $|S|$ with increasing temperature at $25 < T < 70$ K in the polar phase is consistent with the diffusive thermoelectric power, i.e., $S \sim T$. A broad hump of $|S| \sim 200$ K is unusual for a metal but has been observed in other strongly correlated systems such as the single-layer, hole-doped cuprate superconductor [33] and perovskite SrIrO_3 [30]. As displayed in the inset of Fig. 3, $S(T)$ of SrIrO_3 is stunningly like that of LiOsO_3 . Although there is not a good understanding about the broad hump in $S(T)$ at high temperatures, it is interesting to note that the phonon-drag effect is missed in the strongly correlated systems if there is a hump in $S(T)$ at high temperatures. The doping of nonmagnetic Sn^{4+} in $\text{SrIr}_{1-x}\text{Sn}_x\text{O}_3$ leads to a ferromagnetic insulator, which implies that SrIrO_3 is at the crossover of itinerant and localized electronic behavior. There is no obvious hump of $S(T)$ of LaCuO_3 and LaNiO_3 at high temperatures [34], strong correlations as identified by the enhancements of γ and χ_0 are responsible for a much-reduced phonon-drag effect. The phonon-drag effect is restored under high pressure in these two narrow band systems [32]. Another general feature for the systems having the $S(T)$ with a broad hump at high temperatures is that the coefficient A in $S = \pm AT$ as T approaches 0 K is much larger than that the diffusive formula can predict, for example, $A_{\text{measured}} = 0.23 \mu\text{V}/\text{K}^2$ vs $A_{\text{predicted}} = 0.037 \mu\text{V}/\text{K}^2$ for LiOsO_3 . The enhanced A is caused by the complex Fermi surface in the crystal. The Boltzmann gas model can give rise to a $S = \pm AT$ at $T \ll \theta$ and $T > \theta$, but the coefficient A at high temperatures is only $\frac{1}{3}$ of that at low temperatures [31]. Therefore, the broad hump at 200 K in LiOsO_3 may be a part of the crossover between the low temperature $S = -AT$ and the high-temperature $S = -(A/3)T$ at $T > 400$ K. In summary, while increasing the slope in the diffusive formula of thermoelectric $S = \pm AT$ at low temperatures, strong electron correlations suppress the phonon-drag effect and lead to a broad hump of the thermoelectric power at high temperatures in metals.

Here, $S(T)$ of LiOsO_3 becomes field dependent in a narrow range near T_s . The magnetic field suppresses $|S|$, which occurs mainly at $H < 1$ T; almost no field dependence is found for $H > 1$ T. The field dependence provides useful information to understand how the electron-impurity scattering and electron-phonon interaction contribute to the thermoelectric power. Hasegawa *et al.* [35] have modeled the magneto-Seebeck coefficient of bismuth. They found a larger magneto-Seebeck coefficient where the electron-acoustic phonon scattering is dominant; the magneto-Seebeck coefficient becomes negligible in the case of electron-impurity scattering. A very small to negligible field effect on S in LiOsO_3 over the entire temperature range studied suggests that electron-impurity scattering is dominant in the thermoelectric power, which is consistent with the analysis of $S(T)$ based on the diffusive formula above. However, critical fluctuations of the polar phonon mode as revealed by the SHG experiment [15] may contribute to a small magneto-Seebeck effect near T_s .

III. SPECIFIC HEAT AND THE CRITICAL PHENOMENA

Figure 4 displays the result of the specific heat C_p measurement on the LiOsO_3 sample. The transition to the polar

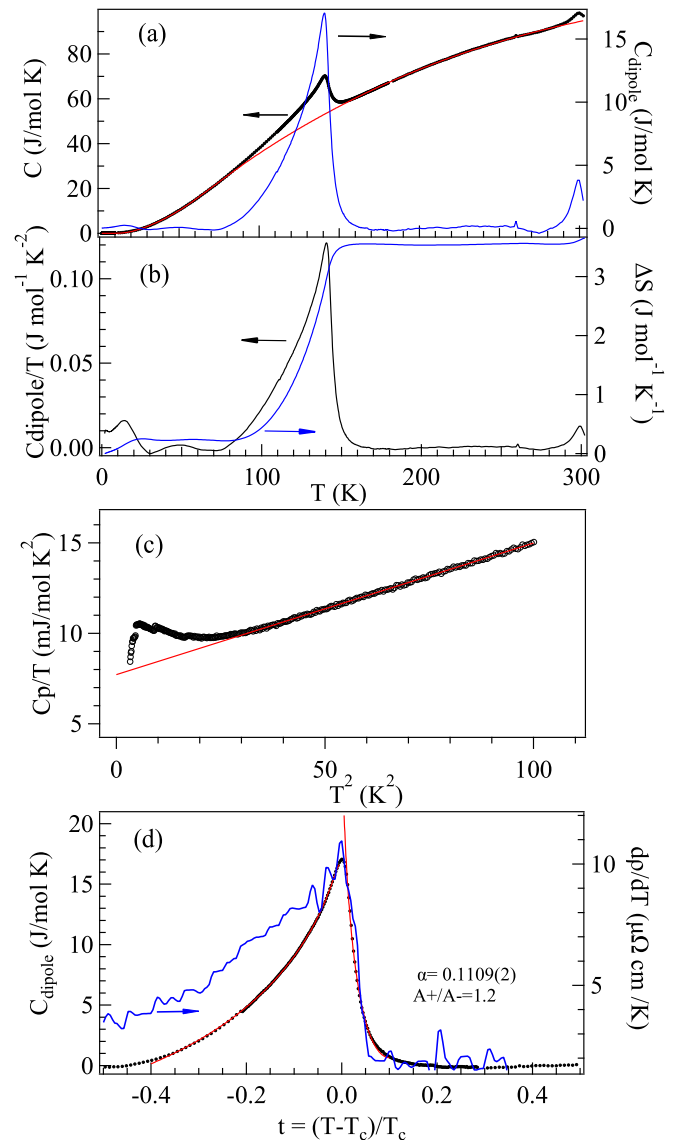


FIG. 4. (a) Temperature dependence of specific heat for LiOsO_3 . Red line in (a) is the C_{latt} obtained by fitting the C_p to the Debye-Einstein model. The contribution to C_p from the dipole ordering C_{dipole} is obtained by subtracting C_{latt} from the original C_p plotted in (a) on the left vertical axis. (b) The entropy change ΔS associated with the transition to the polar phase is calculated by integrating C_{dipole}/T over temperature. (c) The plot of C_p/T vs T^2 ; red line in (c) is the result of a linear fitting to a part of the curve of C_p/T vs T^2 . (d) The plot of C_{dipole} and $d\rho/dT$ vs reduced temperature. Red lines in (d) are the fitting result of C_{dipole} to the formula of the critical behavior. The derivative $d\rho/dT$ from $\rho(T)$ in Fig. 1 is superimposed in (d). In some ferromagnetic metals like SrRuO_3 and Ni, the profile of the C_{mag} anomaly near the ferromagnetic transition T_c matches $d\rho(T)/dT$ well. See the text for the detailed discussion.

phase at T_s creates a clear λ -shaped anomaly in C_p . By excluding the C_p data at temperatures in the vicinity of the phase transition, the lattice contribution to C_p can be fit well to a Debye-Einstein model, as shown in Fig. 4(a). The ΔC_p due to the phase transition can be obtained by subtracting the lattice contribution from C_p . The small anomaly near room temperature is from the puck and the grease used in the C_p

measurement. The entropy change associated with the phase transition in Fig. 4(b) is calculated by $\Delta S = \int \frac{\Delta C_p}{T} dT = 3.5 \text{ J}/(\text{mol K}) = 0.42R$, which is $>0.33R$ in the early report [3]. This discrepancy may be due to the use of a polynomial function in fitting the lattice contribution in the early report. In the plot of C_p/T vs T^2 of Fig. 4(c), the temperature dependence at $5.5 < T < 12 \text{ K}$ can be fit linearly. The fitting gives a $\gamma = 7.72 \text{ mJ}/(\text{mol K}^2)$, which is the same as that in the early report [3]. However, the $\gamma_0 = 6.8 \text{ mJ}/(\text{mol K}^2)$ calculated in the early report is wrong. The authors used the unit of states/cell of DOS at the Fermi energy in their calculation. The correct unit for the DOS in the calculation is states/(eV f.u.) which gives the $\gamma_0 = 2.6 \text{ mJ}/(\text{mol K}^2)$. A large ratio of γ/γ_0 is the first evidence for strongly correlated electrons in LiOsO_3 , which is consistent with the enhancement of paramagnetic susceptibility and an antiferromagnetic ordering at T_N . The low temperature hump in the plot of C_p/T vs T^2 can well be correlated with the magnetic ordering in LiOsO_3 . In addition, the Kadowaki-Woods ratio A/γ^2 [36], A is the parameter in fitting $\rho(T)$ to the Fermi liquid behavior $\rho(T) = \rho_0 + AT^2$, provides information about electron correlations in a metallic system. Comparing with an $A/\gamma^2 \approx 0.4 \mu\Omega \text{ cm mol}^2 \text{ K}^2 \text{ J}^{-2}$ found for regular metals, a much-enhanced $A/\gamma^2 \approx 89 \mu\Omega \text{ cm mol}^2 \text{ K}^2 \text{ J}^{-2}$ obtained for LiOsO_3 suggests strong correlated electrons. Although for a group of materials including strongly correlated electronic systems, a unified Kadowaki-Woods ratio can be derived by adding a material-specific parameter $A/(\gamma^2 f_{dx})$, [37] a comparison of A/γ^2 is still the simplest way to identify the strongly correlated electronic systems.

The critical behavior near the phase transition in the plot of $\Delta C_p = C_{\text{dipole}}$ vs the reduced temperature $t = (T - T_c)/T_c$ in Fig. 4(d) has been analyzed with the formula of conventional theory $C_{\text{mag}} = (A_{\pm}/\alpha)|t|^{-\alpha}(1 + D_{\pm}|t|^{0.5}) + S_0 + S_1 t$. An $\alpha = 0.11$ from the fitting makes the phase transition to a polar phase like a magnetic transition with a three-dimensional (3D) Ising interaction. However, the ratio $A^+/A^- = 1.2$ is significantly larger than the prediction of the 3D Ising model. These data will be useful to test any theories of critical behavior for the ferroelectric transition, especially the ferroelectric transition in a metal. In contrast, by analyzing the Raman data on the 3E_g mode, which is coupled to the polar mode, Jin *et al.* [13] obtained a mean-field behavior at the phase transition. Moreover, the authors obtained a Weiss constant $\theta < T_s$ by fitting the dielectric susceptibility to a Curie-Weiss law. It is highly unusual that a Weiss constant is lower than the transition temperature for either a ferromagnetic or a ferroelectric transition. The absence of critical fluctuations and a reduced Weiss constant in the Raman study have been attributed to the screening effect on the long-range dipole-dipole interaction [13]. Critical fluctuations near T_s found from the specific heat in this paper makes the method used in the Raman study questionable. The dielectric susceptibility in the paraelectric phase is derived from the line width of the 3E_g mode. This method appears unsuitable for the study of critical behavior. Moreover, it is incorrect to say that the presence of itinerant electrons lowers the Weiss constant but not the transition temperature T_s . Critical fluctuations derived from the specific heat study are consistent with the conclusion from the SHG study [15].

Another important observation is that the profile of $\Delta C_p = C_{\text{dipole}}$ in the vicinity of T_s resembles $d\rho/dT$ in Fig. 4(d). The similarity of the critical behavior between $\Delta C_p(T)$ and $d\rho(T)/dT$ has also been reported in the polar metal $\text{Cd}_2\text{Re}_2\text{O}_7$ [38]. For conducting electrons interacting with the ion displacement in the polar semiconductor $\text{Pb}_{1-x}\text{Ge}_x\text{Te}$, a logarithmic increase of the resistivity has been predicted in a model that treats carriers scattering by the two-level system [17]. The model of Kondo-like resistivity has been applied to explain the resistivity upturn at the polar transition in $\text{Ca}_{1-x}\text{Sr}_x\text{TiO}_3$ [20]. The resistivity drop on cooling through T_s in LiOsO_3 resembles the resistivity drop at T_c in metallic ferromagnets such as Ni [39] and SrRuO_3 [21,40] where conduction electrons interact with the array of spins. Moreover, identical critical behaviors in $d\rho(T)/dT$ and $C_{\text{mag}}(T)$ can also be found in these systems. Fisher and Langer [41] have showed that $d\rho/dT$ is proportional to the magnetization energy $|M_0(T)|^2$ at $T < T_c$ and the short-range spin fluctuations at $T > T_c$; therefore, a $d\rho/dT \sim C_{\text{mag}}$ is expected. A dipole analog of the Fisher-Langer theory is needed to explain the resistivity drop on cooling through the polar transition in LiOsO_3 .

IV. MAGNETIC PROPERTY

The magnetic properties of LiOsO_3 were measured with a superconducting quantum interference device magnetometer from Quantum Design. The contribution from the sample's holder was subtracted with the background subtraction function embedded in the Multiview program. The paramagnetic susceptibility $\chi(T)$ of LiOsO_3 in Fig. 5(a) is nearly identical to that reported in the literature [3]. The transition at T_s marks a transformation from a $\chi(T)$ with a $d\chi/dT > 0$ at $T > T_s$ to the Curie-Weiss behavior at $T < T_s$; both behaviors contradict the simple Pauli paramagnetism for free electron gas. In a solid, the band effect introduces a temperature-dependent correction to the Pauli paramagnetic susceptibility χ_0 , i.e., $\chi(T) = \chi_0(1 \pm aT^2)$, $a = \frac{\pi^2}{6} \left\{ \frac{N(\epsilon_F)'}{N(\epsilon_F)} - \left[\frac{N(\epsilon_F)'}{N(\epsilon_F)} \right]^2 \right\}$, where $N(\epsilon_F)$ is the electron DOS at the Fermi energy [42]. A positive sign in the formula corresponds to the case where ϵ_F is located at a minimum of $N(\epsilon)$, whereas a negative sign is applied to the case where ϵ_F is located at a maximum of $N(\epsilon)$. A transition from a phase with $\chi(T) = \chi_0(1 + aT^2)$ to a phase with $\chi(T) = \chi_0(1 - aT^2)$ can create an acute minimum of $\chi(T)$ that resembles the change of $\chi(T)$ for LiOsO_3 on crossing T_s . The behavior change of $\chi(T)$ at T_s can indeed be justified by the change of the DOS from a local maximum at E_F in the polar phase to a local minimum at E_F in the nonpolar phase from a first-principles calculation for LiOsO_3 [7].

Whereas the $\chi(T)$ at $T > T_s$ can be fit perfectly to $\chi(T) = \chi_0(1 + aT^2)$, a good fit for $\chi(T)$ at $T < T_s$ can only be obtained with the formula $\chi(T) = \chi_0(1 - aT^2) + C/T$, as shown in Fig. 5(a). The components of band electron magnetic susceptibility and the Curie-Weiss term in fitting the $\chi(T)$ at $T < T_s$ are shown separately in Fig. 5(b). The Curie-Weiss behavior dominates only at low temperatures. A $\mu_{\text{eff}} = 0.12 \mu_B$ calculated from the Curie-Weiss term is far less than the spin-only value for localized electrons. In the unified theory of the Curie-Weiss law for metals, Moriya [43] has shown

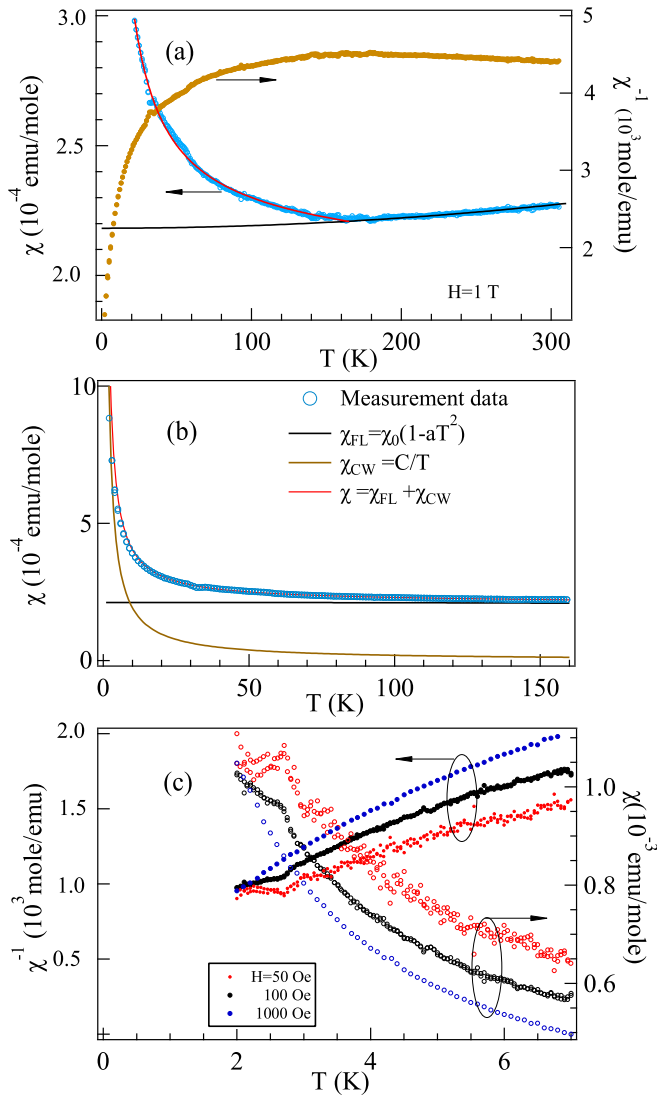


FIG. 5. Temperature dependence of magnetic susceptibility $\chi(T)$ for LiOsO₃ (a) with a high magnetic field, (b) the fitting curve and its components to the $\chi(T)$ in (a), and (c) with low magnetic fields.

that C in the new Curie-Weiss law is not related to the localized moment but the $N(\epsilon_F)$. The transition to the polar phase in LiOsO₃ appears to enhance electron correlations which introduce the ingredient of a Curie-Weiss behavior in the magnetic susceptibility. The effect of strong electron correlations is also reflected in $\chi(T)$ at $T > T_s$. An identical temperature-independent $\chi_0 \approx 2.1 \times 10^{-4}$ emu/mol was obtained from the fittings at both $T > T_s$ and $T < T_s$. With a $\chi_{\text{Pauli}} = 6.4 \times 10^{-5}$ emu/mole calculated based on the band structure of LiOsO₃ [3], a large ratio $\chi_0/\chi_{\text{Pauli}} \approx 3.5$ is a clear indication of strongly correlated electrons in LiOsO₃. Although electron correlations result in enhancements of both χ_0 and γ_0 relative to those based on the band structure, the enhancement of χ_0 in a ferromagnetically coupled system is much more than that in an antiferromagnetically coupled system. For example, $\eta = (\chi_0/\chi_{\text{Pauli}})/(\gamma_{\text{exp}}/\gamma_{\text{cal}}) = 2.45$ is obtained for the Stoner enhanced, $\frac{1}{4}$ -filled LaNiO₃, whereas $\eta = 1$ is for the mass enhanced, $\frac{1}{2}$ -filled LaCuO₃ [34]. An

$\eta = 1.3$ indicates that LiOsO₃ is a strongly correlated system with antiferromagnetic coupling, which is consistent with the t_{2g}^3 electron configuration for Os⁵⁺ in the oxide. Identification of strong correlations in LiOsO₃ from results of specific heat and magnetization measurements is consistent with the conclusion that LiOsO₃ is at the crossover from itinerant to localized electronic behavior from the infrared spectroscopy study [16] and the first-principles calculation [10].

Like Fig. 5(a), the $M(T)$ data originally reported [3] do not show any sign of magnetic ordering in the magnetization measurement at $T > 2$ K. Neutron diffraction did not reveal any magnetic moment $M \geq 0.2 \mu_B$ at $T > 10$ K. In the μ SR experiments on LiOsO₃ with zero field and a longitudinal field, the fluctuations of the moment on Os⁵⁺ slow down < 1.4 K, but the moments remain dynamic down to 0.08 K [44]. The extremely weak magnetization of LiOsO₃ makes it necessary to apply a high magnetic field that may diminish any features deviating from the Curie-Weiss behavior at low temperatures. At a magnetic field < 100 Oe, the magnetic response from the LiOsO₃ sample is in the same level as the contribution from the sample holder in the magnetization measurement with the MPMS. Measurements with the background subtraction function at low magnetic fields in this paper reveal a well-defined dipole in a scan. The $M(T)$ for $H \leq 100$ Oe show a weak anomaly ~ 3 K in Fig. 5(c). The cusp feature and the overlap between field cool and zero-field cool may suggest an antiferromagnetic ordering without spin canting. The magnetic ordering may also be the primary source for the hump at low temperatures in the plot of C_p/T vs T^2 in Fig. 4(c). Since the anomaly ~ 3 K only appears at low fields, we cannot rule out the possibility that it comes from a tiny impurity phase in the sample. It is also worth noting that all possible impurity phases such as Os metal and OsO₂ do not show any anomalies in their $M(T) \sim 3$ K. It is also important to note that the magnetic susceptibility of LiOsO₃ is field dependent, at least for $H \leq 1000$ Oe in Fig. 5(c). A nonlinear $M(H)$ of LiOsO₃ indicates that spins undergo ordering even at $T > 3$ K.

It remains an interesting dialog whether LiOsO₃ becomes magnetic. The enhanced γ_0 and χ_0 and the Kadowaki-Woods ratio indicate clearly that LiOsO₃ is a strongly correlated system. The anomaly in $M(T) \sim 3$ K and the broad hump at low temperatures in the plot of C_p/T vs T^2 seem to support magnetic ordering. By using the LSDA + U method, He [38] predicted that the chemically stoichiometric LiOsO₃ should be a G-type antiferromagnetic semiconductor. The magnetism disappears for the Li-deficient Li_{1-x}OsO₃, which is a metal. The lithium deficiency has been indeed verified in the LiOsO₃ sample by refining neutron powder diffraction [3]. On the other hand, the effect of the spin-orbit coupling is generally to suppress any magnetic orderings, as calculated for LiOsO₃ by Zhang *et al.* [45]. LiOsO₃ should also be a Hund's metal from the t_{2g}^3 configuration. The role of a Hund's coupling J_H is to make a frustrated spin or spin frozen state [24,46]. The weak anomaly found in $\chi(T) \sim 3$ K at a low magnetic field and a nonlinear $M(H)$ at low temperatures may result from the competition among electron-electron correlations, the spin-orbit coupling, and the Hund's coupling. It is also important to note that the chemical stoichiometry in LiOsO₃ may alter the magnetic property. Further study is needed to have a

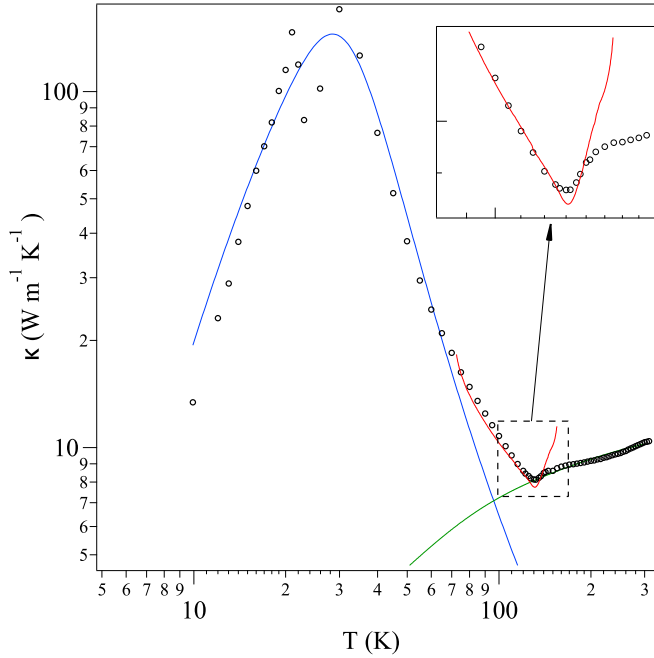


FIG. 6. Temperature dependence of thermal conductivity for LiOsO₃; the inset is a zoom-in plot showing the detail near the transition at T_s . Lines in the plot are the fitting results to the Debye formula at $T < 50$ K and the general formula of κ (basically from C_p) at $T > 160$ K; the line in the vicinity of T_s is scaled from the Stern's formula of critical behavior for κ .

complete understanding of the magnetic state in LiOsO₃ at low temperatures.

Ferroelectric LiOsO₃ with strongly correlated electrons may exhibit a unique nonlinear optical property, as predicted by Fu [47], as factors like parity breaking and strong spin-orbit coupling are considered. Whereas whether an antiferromagnetic order breaks the time reversal symmetry remains under debate, it would be interesting to explore the optical properties < 2.4 K in LiOsO₃ where both inversion symmetry and time reversal symmetry are broken.

V. THERMAL CONDUCTIVITY

The measurement of thermal conductivity $\kappa(T)$ of LiOsO₃ was made by the steady-state method on small bars of polycrystalline samples. The results are highly repeatable. Since LiOsO₃ is a metal, the up-bound contribution κ_e from electrons to the total thermal conductivity can be evaluated by the Wiedemann-Franz law based on the resistivity data in Fig. 1. LiOsO₃ is a bad metal, so that κ_e is negligibly small in comparison with the lattice contribution κ_{ph} . Figure 6 shows the temperature dependence of κ_{ph} below room temperature. A $\kappa = 10.4$ W m⁻¹ K⁻¹ at room temperature is at the high-end value among the ABO₃ oxides [48–54]; but the temperature dependence of κ indicates a glassy thermal conductor in the nonpolar phase. A relatively sharp minimum of $\kappa(T)$ is clearly visible in the vicinity of the critical temperature T_s followed by a huge peak centering at 30 K. The phonon thermal conductivity of $\kappa(T)$ in LiOsO₃ < 50 K is comparable with that of a diamagnetic LaGaO₃ crystal [53], but the κ of LiOsO₃

TABLE I. The fitting parameters in the curve fitting of $\kappa(T)$ in LaGaO₃ and LiOsO₃ to the Debye formula in Eq. (2).

	LaGaO ₃	LiOsO ₃
ν (m/s)	4230	4022
Θ_D (K)	554	470
A (s ³)	4.705×10^{-44}	1.88×10^{-44}
B (K ⁻¹ s ²)	6.351×10^{-31}	5.7×10^{-30}
b	6.031	2.36
L (m)	1.0×10^{-4}	8.8×10^{-6}

peaking at a higher temperature than that for LaGaO₃ crystal means that the crystal quality of LiOsO₃ is slightly low relative to that of the LaGaO₃ crystal used in an early study.

The phonon thermal conductivity of LiOsO₃ below T_s can be essentially described by a gas model overall. The large peak of κ_{ph} at low temperatures reflects the phonon-phonon, phonon-impurity, phonon-grain boundary scatterings; these scatterings are covered in the Debye formula [55]:

$$\kappa_{ph}(T) = \left(\frac{k_B}{2\pi^2\nu} \right) \left(\frac{k_B}{\hbar} \right)^3 T^3 \int_0^{\Theta_D/T} \frac{x^4 e^x}{(e^x - 1)^2} \tau(\omega, T) dx, \quad (2)$$

where $x = \hbar\omega/k_B T$, ν is the phonon velocity, and $\tau(\omega, T)$ is the relaxation time of a phonon, which can be expressed as

$$\tau^{-1} = \frac{\nu}{L} + A\omega^4 + B\omega^3 T e^{(-\Theta_D/bT)}. \quad (3)$$

The first term in Eq. (3) is related to phonon scattering at the boundary of the sample, the second is about scattering at defects, and the third is the phonon-phonon scattering. The phonon-phonon scattering dominates κ_{ph} at high temperatures, whereas the effects due to scatterings at the boundary of the sample or at impurities become obvious at low temperatures. The Debye temperature $\Theta_D = 470$ K used in the fitting is from the specific heat result. As superimposed in Fig. 6, the fitting curve to the Debye formula matches the essential feature of the κ_{ph} peak at low temperatures, and the fitting parameters are given in Table I. One of the remarkable differences of κ_{ph} for LiOsO₃ in comparison with LaGaO₃ and other crystalline oxides [54] is a surprisingly small L (for the boundary scattering) in the first term of Eq. (3). Since the textured crystal used consists of large-sized (~ 200 μ m) crystal grains, the boundary scattering in the sample should not be much different from other single-crystal oxides. In a ferroelectric crystal, phonons may experience extra scatterings at the ferroelectric domain boundaries, which has been demonstrated in other ferroelectric oxides LiTaO₃ [54] and BiFeO₃ [56].

The glassy κ_{ph} of LiOsO₃ occurs at $T > T_s$. The phonon thermal conductivity can be generally expressed by $\kappa_{ph} = \frac{1}{3} C_{ph} \nu l$, where $C_{ph} \sim C_p$ is the lattice heat capacity, ν is the sound velocity, and l is the phonon mean free path. A glassy κ_{ph} indicates that the mean free path l is limited to the phonon-phonon scattering at the level of interatomic distance. In this case, the temperature dependence of κ_{ph} is basically determined by $C_{ph}(T)$ [55]. A curve of $\kappa = \kappa_{ph}$ is superimposed in Fig. 6, which indeed matches the general trend of the glassy κ_{ph} at $T > T_s$ very well. The randomness of Li ions

distributed on the $12c$ position in the crystal structure is responsible for the phonon scattering at the level of interatomic distance in the nonpolar phase. In contrast, the phonon thermal conductivity has been found in both the paraelectric and ferroelectric phases in the displacive transition of PbTiO_3 [57]. The remarkable transition from a glassy κ_{ph} to a phononlike κ_{ph} at T_s is solid proof of an order-disorder transition in LiOsO_3 , as a similar $\kappa(T)$ has been found in other ferroelectrics [58] where an order-disorder transition occurs. It should be noticed that a glassy $\kappa_{\text{ph}} \sim 10 \text{ W m}^{-1} \text{ K}^{-1}$ at room temperature for LiOsO_3 is much higher than a typical glassy κ_{ph} seen in other oxides [52,53]. This difference could be accounted for by a relatively high sound velocity v in LiOsO_3 .

The κ_{ph} of LiOsO_3 undergoes a clear dip in the vicinity of T_s , which has not been seen in any ferroelectric insulators to our knowledge [57–59]. The data will be useful to test any microscopic models to describe the influence of critical fluctuations near a ferroelectric transition on thermal conductivity. It is interesting to compare the influence of dipole critical fluctuations on thermal conductivity with that by spin fluctuations. In magnetic insulators, spin critical fluctuations near a spin-ordering temperature disturb the heat transportation via phonons. Stern [60] has taken the Heisenberg exchange interaction, which is modulated by lattice vibrations, to account for a dip of $\kappa(T)$ commonly found in magnetic insulators. The effect of spin fluctuations on κ_{ph} enters the second term in Eq. (3) as $(B_1 + B_2 T^2 C_{\text{mag}}) \omega^4$, where B_1 and B_2 are constants, and C_{mag} is the heat capacity for spins. For $x < 1$ in Eq. (2), a $\kappa_{\text{ph}} \propto (B_1 + B_2 T^2 C_{\text{mag}})^{-3/4}$ can be obtained. By taking the C_{mag} from the specific heat measurement, Stern [60] and later Lewis and Saunders [61] can account for a dip of κ_{ph} near T_N qualitatively. Under an assumption that dipoles act as spins in terms of the effect of critical fluctuations on the phonon transport, we can have a dipole version of Stern's formula $\kappa_{\text{ph}} = (B_1 + B_2 T^2 C_{\text{dipole}})^{-3/4}$ in the narrow temperature range around T_c . As shown in Fig. 6 and more clearly in the inset, the simulated κ_{ph} can account stunningly well for the essential feature of the critical behavior of κ_{ph} near T_c .

One may be curious why a dip of $\kappa(T)$ at T_c has not been found in other ferroelectrics like KH_2PO_4 and KH_2AsO_4 , which also show a glassy $\kappa(T)$ in the nonpolar phase and a phonon $\kappa(T)$ in the polar phase [58]. These early measurements do not have a sufficiently high number of sampling

points near T_c . Most importantly, these ferroelectrics are insulators. The dip of $\kappa(T)$ found in LiOsO_3 may be related to the interplay between free electrons and critical fluctuations of dipoles.

VI. CONCLUSIONS

LiOsO_3 provides an excellent example to study how itinerant electrons respond to dipole dynamics, fluctuations, and ferroelectric ordering; it is a rare ferroelectric metal with strongly correlated electrons. LiOsO_3 is an n -type metal in both polar and nonpolar phases. While the monotonic temperature dependence of the thermoelectric power at $T < T_s$ is close to the behavior of the diffusive formula, the slope is significantly enhanced relative to the prediction based on the band structure. The thermoelectric power at $T > T_s$ cannot be accounted for by any models for metals. Strong correlations of electrons in LiOsO_3 are reflected in enhancements of γ and χ_0 relative to the predictions from the band structure as well as in the Kadowaki-Woods ratio. The ratio $(\chi_0/\chi_{\text{Pauli}})/(\gamma_{\text{exp}}/\gamma_{\text{cal}}) = 1.3$ indicates an antiferromagnetic coupling in the strongly correlated LiOsO_3 . As for the effect of dipole ordering to the lattice dynamics, the thermal conductivity κ shows a remarkable change from a glassy to a phononlike phase at the nonpolar-to-polar transition, which indicates conclusively an order-disorder transition at T_s . The analysis of phonon thermal conductivity in the polar phase reveals that phonons are scattered at ferroelectric domain boundaries in addition to grain boundaries. Like ferromagnetic metals, the profile of $d\rho/dT$ matches that of $\Delta C = C_p - C_{\text{latt}}$ near T_s in LiOsO_3 . The influence of critical fluctuations of dipoles on the thermal conductivity resembles that in antiferromagnetic insulators. These findings are useful to test theories of critical behaviors for ferroelectric metals.

ACKNOWLEDGMENTS

This paper was supported by the National Science Foundation, Grant No. DMR-1905598. K.Y. was supported in part by a research grant from Innovative Science and Technology Initiative for Security, ATLA (Grant No. JPJ004596), Japan, and JSPS KAKENHI (Grant No. JP20H05276), Japan.

-
- [1] J. C. Slater, The Lorentz correction in barium titanate, *Phys. Rev.* **78**, 748 (1950).
 - [2] P. W. Anderson and E. I. Blount, Symmetry Considerations on Martensitic Transformations—Ferroelectric Metals, *Phys. Rev. Lett.* **14**, 217 (1965).
 - [3] Y. G. Shi, Y. F. Guo, X. Wang, A. J. Princep, D. Khalyavin, P. Manuel, Y. Michiue, A. Sato, K. Tsuda, S. Yu, M. Arai, Y. Shirako, M. Akaogi, N. L. Wang, K. Yamaura, and A. T. Boothroyd, A ferroelectric-like structural transition in a metal, *Nat. Mater.* **12**, 1024 (2013).
 - [4] V. Keppens, Structural transitions ‘ferroelectricity’ in a metal, *Nat. Mater.* **12**, 952 (2013).
 - [5] P. Liu, J. He, B. Kim, S. Khmelevskyi, A. Toschi, G. Kresse, and C. Franchini, Comparative *ab initio* study of the structural, electronic, magnetic, and dynamical properties of LiOsO_3 and NaOsO_3 , *Phys. Rev. Mater.* **4**, 045001 (2020).
 - [6] G. Giovannetti and M. Capone, Dual nature of the ferroelectric and metallic state in LiOsO_3 , *Phys. Rev. B* **90**, 195113 (2014).
 - [7] H. Sim and B. G. Kim, First-principles study of octahedral tilting and ferroelectric-like transition in metallic LiOsO_3 , *Phys. Rev. B* **89**, 201107(R) (2014).
 - [8] H. M. Liu, Y. P. Du, Y. L. Xie, J. M. Lin, C. G. Duan, and X. Wan, Metallic ferroelectricity induced by anisotropy unscreened Coulomb interaction in LiOsO_3 , *Phys. Rev. B* **91**, 064104 (2015).
 - [9] W. C. Yu, X. Zhou, F. C. Chuang, S. A. Yang, H. Lin, and A. Bansil, Nonsymmorphic cubic Dirac point and crossed nodal

- rings across the ferroelectric phase transition in LiOsO_3 , *Phys. Rev. Mater.* **2**, 051201(R) (2018).
- [10] D. Springer, B. Kim, P. Liu, S. Khmelevskiy, S. Adler, M. Capone, G. Sangiovanni, C. Franchini, and A. Toschi, Osmates on the Verge of a Hund's-Mott Transition: The Different Fates of NaOsO_3 and LiOsO_3 , *Phys. Rev. Lett.* **125**, 166402 (2020).
- [11] H. J. Xiang, Origin of polar distortion in LiNbO_3 -type "ferroelectric" metals: role of A-site instability and short-range interactions, *Phys. Rev. B* **90**, 094108 (2014).
- [12] F. Jin, A. M. Zhang, J. T. Ji, K. Liu, L. Wang, Y. G. Shi, Y. Tian, X. L. Ma, and Q. M. Zhang, Raman phonons in the ferroelectric-like metal LiOsO_3 , *Phys. Rev. B* **93**, 064303 (2016).
- [13] F. Jin, L. Wang, A. M. Zhang, J. T. Ji, Y. G. Shi, X. Q. Wang, R. Yu, J. D. Zhang, E. W. Plummer, and Q. M. Zhang, Raman interrogation of the ferroelectric phase transition in polar metal LiOsO_3 , *Proc. Natl. Acad. Sci. USA* **116**, 20322 (2019).
- [14] N. J. Laurita, A. Ron, Jun-Yi Shan, D. Puggioni, N. Z. Koocher, K. Yamaura, Y. Shi, J. M. Rondinelli, and D. Hsieh, Evidence for the weakly coupled electron mechanism in an Anderson-Blount polar metal, *Nat. Commun.* **10**, 3217 (2019).
- [15] J. Y. Shan, A. de la Torre, N. J. Laurita, L. Zhao, C. D. Dashwood, D. Puggioni, C. X. Wang, K. Yamaura, Y. Shi, J. M. Rondinelli, and D. Hsieh, Evidence for an extended critical fluctuation region above the polar ordering transition in LiOsO_3 , *Phys. Rev. Research* **2**, 033174 (2020).
- [16] I. Lo Vecchio, G. Giovannetti, M. Autore, P. Di Pietro, A. Perucchi, J. F. He, K. Yamaura, M. Capone, and S. Lupi, Electronic correlations in the ferroelectric metallic state of LiOsO_3 , *Phys. Rev. B* **93**, 161113(R) (2016).
- [17] S. Katayama, S. Maekawa, and H. Fukuyama, Kondo-like effect of orbital motion on resistivity in $\text{Pb}_{1-x}\text{Ge}_x\text{Te}$, *J. Phys. Soc. Jpn.* **56**, 697 (1987).
- [18] M. D. Glinchuk and I. V. Kondakova, Ruderman-Kittel-like interaction of electric dipoles in systems with carriers, *Phys. Status Solidi B* **174**, 193 (1992).
- [19] M. Itoh, R. Wang, Y. Inaguma, T. Yamaguchi, Y. J. Shan, and T. Nakamura, Ferroelectricity Induced by Oxygen Isotope Exchange in Strontium Titanate Perovskite, *Phys. Rev. Lett.* **82**, 3540 (1999).
- [20] J. Wang, L. Yang, C. W. Rischau, Z. Xu, Z. Ren, T. Lorenz, J. Hemberger, X. Lin, and K. Behnia, Charge transport in a polar metal, *NPJ Quantum Materials* **4**, 61 (2019).
- [21] P. B. Allen, H. Berger, O. Chauvet, L. Forro, T. Jarlborg, A. Junod, B. Revaz, and G. Santi, Transport properties, thermodynamic properties, and electronic structure of SrRuO_3 , *Phys. Rev. B* **53**, 4393 (1996).
- [22] P. B. Allen and W. W. Schulz, Bloch-Boltzmann analysis of electrical transport in intermetallic compounds— ReO_3 , BaPbO_3 , CoSi_2 , and Pd_2Si , *Phys. Rev. B* **47**, 14434 (1993).
- [23] J. K. Hulm and B. B. Goodman, Superconducting properties of rhenium, ruthenium, and osmium, *Phys. Rev.* **106**, 659 (1957).
- [24] L. de' Medici, J. Mravlje, and A. Georges, Janus-Faced Influence of Hund's Rule Coupling in Strongly Correlated Materials, *Phys. Rev. Lett.* **107**, 256401 (2011).
- [25] F. Hardy, A. E. Böhmer, D. Aoki, P. Burger, T. Wolf, P. Schweiss, R. Heid, P. Adelman, Y. X. Yao, G. Kotliar, J. Schmalian, and C. Meingast, Evidence of Strong Correlations and Coherence-Incoherence Crossover in the Iron Pnictide Superconductor KFe_2As_2 , *Phys. Rev. Lett.* **111**, 027002 (2013).
- [26] Z. Fisk and G. W. Webb, Saturation of the High-Temperature Normal-State Electrical Resistivity of Superconductors, *Phys. Rev. Lett.* **36**, 1084 (1976).
- [27] A. J. Millis, Jun Hu, and S. Das Sarma, Resistivity Saturation Revisited: Results from a Dynamical Mean Field Theory, *Phys. Rev. Lett.* **82**, 2354 (1999).
- [28] E. I. Paredes Aulestia, Y. W. Cheung, Y.-W. Fang, J. He, K. Yamaura, K. T. Lai, S. K. Goh, and H. Chen, Pressure-induced enhancement of non-polar to polar transition temperature in metallic LiOsO_3 , *Appl. Phys. Lett.* **113**, 012902 (2018).
- [29] J. J. Gao, S. Y. Fu, K. Yamaura, J. F. Lin, and J. S. Zhou, Room-temperature polar metal stabilized under high pressure, *Phys. Rev. B* **101**, 220101(R) (2020).
- [30] Q. Cui, J. G. Cheng, W. Fan, A. E. Taylor, S. Calder, M. A. McGuire, J. Q. Yan, D. Meyers, X. Li, Y. Q. Cai, Y. Y. Jiao, Y. Choi, D. Haskel, H. Gotou, Y. Uwatoko, J. Chakhalian, A. D. Christianson, S. Yunoki, J. B. Goodenough, and J. S. Zhou, Slater Insulator in Iridate Perovskites with Strong Spin-Orbit Coupling, *Phys. Rev. Lett.* **117**, 176603 (2016).
- [31] D. K. C. MacDonald, *Thermoelectricity: An Introduction to the Principles* (John Wiley & Sons, New York, 1962).
- [32] J. S. Zhou, W. Archibald, and J. B. Goodenough, Pressure dependence of thermoelectric power in $\text{La}_{1-x}\text{Nd}_x\text{CuO}_3$, *Phys. Rev. B* **57**, R2017 (1998).
- [33] J. S. Zhou and J. B. Goodenough, Thermoelectric power in single-layer copper oxides, *Phys. Rev. B* **51**, 3104 (1995).
- [34] J. S. Zhou, L. G. Marshall, and J. B. Goodenough, Mass enhancement versus Stoner enhancement in strongly correlated metallic perovskites: LaNiO_3 and LaCuO_3 , *Phys. Rev. B* **89**, 245138 (2014).
- [35] Y. Hasegawa, T. Komine, Y. Ishikawa, A. Suzuki, and H. Shirai, Numerical calculation of magneto-Seebeck coefficient of bismuth under a magnetic field, *Jpn. J. Appl. Phys.* **43**, 35 (2004).
- [36] K. Kadowaki and S. B. Woods, Universal relationship of the resistivity and specific heat in heavy-Fermion compounds, *Solid State Commun.* **58**, 507 (1986).
- [37] A. C. Jacko, J. O. Fjærestad, and B. J. Powell, A unified explanation of the Kadowaki-Woods ratio in strongly correlated metals, *Nat. Phys.* **5**, 422 (2009).
- [38] J. He, Metallic ferroelectricity and superconductivity in the transition metal oxide pyrochlore $\text{Cd}_2\text{Re}_2\text{O}_7$, Ph.D. thesis, University of Tennessee, Knoxville, 2004.
- [39] P. P. Craig, W. I. Goldberg, T. A. Kitchens, and J. I. Budnick, Transport Properties at Critical Points: The Resistivity of Nickel, *Phys. Rev. Lett.* **19**, 1334 (1967).
- [40] D. Kim, B. L. Zink, F. Hellman, S. McCall, G. Cao, and J. E. Crow, Mean-field behavior with Gaussian fluctuations at the ferromagnetic phase transition of SrRuO_3 , *Phys. Rev. B* **67**, 100406(R) (2003).
- [41] M. E. Fisher and J. S. Langer, Resistive Anomalies at Magnetic Critical Points, *Phys. Rev. Lett.* **20**, 665 (1968).
- [42] P. Mohn, *Magnetism in the Solid State, An Introduction* (Springer, Berlin, 2006).
- [43] T. Moriya, Spin fluctuations and a unified picture of magnetism, in *Electron Correlation and Magnetism in Narrow-Band Systems*, edited by T. Moriya (Springer-Verlag, Berlin, Heidelberg, New York, 1981).
- [44] F. K. K. Kirschner, F. Lang, F. L. Pratt, T. Lancaster, Y. Shi, Y. Guo, A. T. Boothroyd, and S. J. Blundell, Static and fluctuating

- magnetic moments in the ferroelectric metal LiOsO_3 , *JPS Conf. Proc.* **21**, 011013 (2018).
- [45] Y. Zhang, J. Gong, C. Li, L. Lin, Z. Yan, S. Dong, and J.-M. Liu, Possible origin of the absence of magnetic order in LiOsO_3 : spin-orbit coupling controlled ground state, *Phys. Status Solidi RRL* **12**, 1800396 (2018).
- [46] P. Werner, E. Gull, M. Troyer, and A. J. Millis, Spin Freezing Transition and Non-Fermi-Liquid Self-Energy in a Three-Orbital Model, *Phys. Rev. Lett.* **101**, 166405 (2008).
- [47] L. Fu, Parity-Breaking Phases of Spin-Orbit-Coupled Metals with Gyrotropic, Ferroelectric, and Multipolar Orders, *Phys. Rev. Lett.* **115**, 026401 (2015).
- [48] J. Q. Yan, J. S. Zhou, and J. B. Goodenough, Bond-length fluctuations and the spin-state transition in LCoO_3 ($L = \text{La, Pr, and Nd}$), *Phys. Rev. B* **69**, 134409 (2004).
- [49] J. S. Zhou and J. B. Goodenough, Dynamic Jahn-Teller distortions and thermal conductivity in $\text{La}_{1-x}\text{Sr}_x\text{MnO}_3$ crystals, *Phys. Rev. B* **64**, 024421 (2001).
- [50] J. S. Zhou and J. B. Goodenough, Probing structural inhomogeneities induced by exchange striction above T_N in antiferromagnetic perovskites, *Phys. Rev. B* **66**, 052401 (2002).
- [51] J. S. Zhou, J. B. Goodenough, and B. Dabrowski, Transition from Curie-Weiss to enhanced Pauli paramagnetism in RNiO_3 ($R = \text{La, Pr, } \dots \text{ Gd}$), *Phys. Rev. B* **67**, 020404(R) (2003).
- [52] J. Q. Yan, J. S. Zhou, and J. B. Goodenough, Unusually Strong Orbit-Lattice Interactions in the RVO_3 Perovskites, *Phys. Rev. Lett.* **93**, 235901 (2004).
- [53] J. G. Cheng, Y. Sui, J. S. Zhou, J. B. Goodenough, and W. H. Su, Transition from Orbital Liquid to Jahn-Teller Insulator in Orthorhombic Perovskites RTiO_3 , *Phys. Rev. Lett.* **101**, 087205 (2008).
- [54] E. Langenberg, E. Ferreiro-Vila, V. Leborán, A. O. Fumega, V. Pardo, and F. Rivadulla, Analysis of the temperature dependence of the thermal conductivity of insulating single crystal oxides, *APL Materials* **4**, 104815 (2016).
- [55] B. Berman, *Thermal Conductivity in Solids* (Oxford University Press, London, 1976).
- [56] P. E. Hopkins, C. Adamo, L. Ye, B. D. Huey, S. R. Lee, D. G. Schlom, and J. F. Ihlefeld, Effects of coherent ferroelastic domain walls on the thermal conductivity and Kapitza conductance in bismuth ferrite, *Appl. Phys. Lett.* **102**, 121903 (2013).
- [57] I. Yoshida, Thermal conduction in ferroelectric ceramics, *J. Phys. Soc. Jpn.* **15**, 2211 (1960).
- [58] Y. Suemune, Thermal conductivity of some ferroelectric crystals with hydrogen bonds, *J. Phys. Soc. Jpn.* **22**, 735 (1967).
- [59] M. Tachibana, T. Kolodiazny, and E. Takayama-Muromachi, Thermal conductivity of perovskite ferroelectrics, *Appl. Phys. Lett.* **93**, 092902 (2008).
- [60] H. Stern, Thermal conductivity at the magnetic transition, *J. Phys. Chem. Solids* **26**, 153 (1965).
- [61] F. B. Lewis and N. H. Saunders, The thermal conductivity of NiO and CoO at the Neel temperature, *J. Phys. C. Solid State Phys.* **6**, 2525 (1973).